J. Biochem. 2011;149(5):569–580 doi:10.1093/jb/mvr007

JB THE JOURNAL OF BIOCHEMISTRY

Conformational analysis of human serum albumin and its non-enzymatic glycation products using monoclonal antibodies

Received November 15, 2010; accepted January 12, 2011; published online January 21, 2011

Keigo Saito[1,2,*], Kuniko Hamano[1,2,*], Masatoshi Nakagawa[1,†], Keiko Yugawa[3], Jin Muraoka[3], Hiroyoshi Kuba[2], Koji Furukawa[2,4] and Takachika Azuma[1,‡]

[1]Research Institute for Biological Sciences (RIBS), Tokyo University of Science (TUS), 2669, Yamazaki, Noda, Chiba 278-0022; [2]Age Dimension Research Center, National Institute of Advanced Industrial Science and Technology (AIST), AIST Tsukuba Central 6, 1-1-1 Higashi, Tsukuba, Ibaraki 305-8566; [3]Bioscience Technology Development Office, Panasonic Corporation 3-4, Hikaridai, Seika-cho, Soraku, Kyoto 619-0237; and [4]Medical Research Institute, Tokyo Medical and Dental University, 1-5-45, Yushima, Bunkyo-ku, Tokyo 113-8510, Japan

*These authors contributed equally to this work.
†Present address: Masatoshi Nakagawa, Abbott Japan Co., Ltd., 278, Matsuhidai, Matsudo, Chiba 270-2214, Japan

‡Takachika Azuma, Research Institute for Biological Sciences (RIBS), Tokyo University of Science (TUS), 2669, Yamazaki, Noda, Chiba 278-0022, Japan. Tel: +81 4 7121 4082, Fax: +81 4 7121 4039, email: tazuma@rs.noda.tus.ac.jp

Monoclonal antibodies (mAbs) were prepared to analyse the conformation of human serum albumin (HSA) and its non-enzymatic glycation (NEG) products. We first determined the epitopes of the mAbs using HSA subdomains expressed on the surface of yeast. Each mAb was classified as belonging to one of two groups; Type I mAbs which recognized a single subdomain structure and Type II mAbs which bound to plural subdomains. We analysed the pH-dependent conformational change in HSA. We found that one Type II mAb, HAy2, detected the normal to base form (N-B) transition while the other did not, suggesting that N-B transition occurred around Domain I accompanied by topological isomerization of subdomains without changing the subdomain structure itself. Next, we analysed the conformations of the NEG products. Since all mAbs reacted with the early NEG products, no structural change was thought to have occurred in the early NEG products. On the other hand, only a Type I mAb, HAy1, had full binding activity with the advanced glycation end products (AGE) while the other mAbs had lost or had diminished activity, suggesting that the over-all tertiary structure of HSA was altered except for a subdomain, sDOM Ia, in AGE.

Keywords: antibody recognition/human serum albumin/N-B transition/non-enzymatic glycation/yeast surface display.

Abbreviations: AGE, advanced glycated end product; Ab, antibody; CD, circular dichroism; ΔH, enthalpy change; ΔS, entropy change; ΔG, Gibb's free energy change; DOM, domain; ELISA, enzyme-linked immunosorbent assay; FACS, fluorescence activated flow cytometry; gHSA, glycated HSA; HSA, human serum albumin; HSA_{bio}, biotinylated HSA; ITC, isothermal titration calorimetry; mAb, monoclonal antibody; NEG, non-enzymatic glycation; PBS, phosphate-buffered saline; PBST, PBS containing 0.1% Tween-20; PE, phycoerythrin; sDOM, subdomain; SD-CAA, synthetic dextrose medium with casamino acids; YSD, yeast surface display.

Human serum albumin (HSA) is the most abundant protein in blood and plays an important role in controlling colloidal osmotic pressure and pH in the blood circulation. HSA also acts as a transporter of endogenous molecules such as fatty acids, hemin, bilirubin and some metals (*1*). Structural studies showed that HSA is composed of three homologous domains, referred to as DOM I, DOM II and DOM III (*2*–*4*), and has two binding sites, binding site I and II (*5*). Binding site I which consists of DOM I and a portion of DOM II, can bind to various drugs (*2*). Conformational change in HSA as a result of ligand binding has been studied extensively using various physicochemical methods including X-ray crystallography (*6*–*9*). These studies have shown that DOM I undergoes conformational change when ligands bind to site I and this was thought to be related to its transporter function.

Non-enzymatic glycosylation (NEG) is known to occur during long-term incubation with glucose at ε-amino groups of lysine residues in various proteins (*10*). This reaction is initiated by the reversible formation of a Schiff base adduct that undergoes rearrangement to form more stable Amadori products, which then undergo a series of rearrangements and reactions to yield various protein adducts collectively termed advanced glycation end products (AGEs) (*11*). The process of glycation and the formation of AGEs, accompanied by protein aggregation and insolubilization, is thought to be involved in the structural and functional changes that proteins undergo *in vivo* during ageing and as part of the long-term complications of diabetes (*12*). However, only limited information is available regarding the effects of these modifications on secondary or tertiary protein structure (*13*, *14*).

Antibodies (Abs) have previously been utilized for probing the folding of proteins (*15*, *16*). These studies showed that Abs can identify conformational variants that occur during protein folding. Our interest lies in using Abs to detect the fine conformational changes in proteins, which may relate to protein function.

In particular, in the case of multidomain proteins such as HSA, changes in domain–domain interactions were expected to modify function by altering the conformation of the ligand-binding sites (*17*). For this purpose, we generated an array of anti-HSA monoclonal Abs (mAbs) and examined their interactions with HSA. For a precise understanding of these interactions, information on the epitopes recognized by the mAbs was considered critical. We therefore employed a yeast surface display (YSD) system for mapping the epitopes (*18*, *19*). Individual domains or plural domains were expressed on the yeast surface on which the binding of anti-HSA mAbs was analysed using fluorescence activated flow cytometry (FACS). Interactions between HSA and anti-HSA mAbs were measured using isothermal titration calorimetry (ITC) and an enzyme-linked immunosorbent assay (ELISA) system. ITC has been widely used for thermodynamic measurement of protein–protein interactions including antigen (Ag)–Ab interactions. Experimental binding isotherms of Ag–Ab interactions can be described precisely by means of such parameters as the enthalpy change (ΔH) and the association constant (K_a), which in turn allow for calculation of Gibb's free energy change (ΔG) and entropy change (ΔS) (*20*). These thermodynamic parameters were used to provide information on the chemical nature of the amino acid residues involved in the interactions.

Using the anti-HSA mAbs that were well-characterized in terms of epitope recognition and binding thermodynamics, we first addressed the question of whether they could detect and define the fine conformational changes in HSA which are known to occur at both an acidic (below pH 4) and basic (above pH 7) pH. The former change was referred to as 'normal form (N) to faster migration form (F) transition' (N-F transition) and the latter as 'normal form (N) to basic form (B) transition' (N-B transition) (*3*, *21*). We studied N-B transition in detail since it occurs under physiological conditions and has not as yet been well characterized in terms of the domains involved in this transition. Next, we extended our study to explore conformational change induced by NEG. This post-translational modification was considered to contribute to long-term diabetic complications (*12*). The association of AGEs with a variety of pathologies has aroused in much interest in the role played by NEG products and AGEs in the pathology of diabetes and the chemical structure of glycated HSA (gHSA) has been studied using mass spectroscopy (*12*, *22–25*). However, there is little information on whether NEG influences or changes the local secondary structure of a protein or its over-all tertiary structure including that resulting from interdomain interactions.

Our intention in the present study was to use mAbs to dissect conformational changes in HSA. Since HSA is a major serum protein, alterations in its conformation could serve as an indicator of changes within various body tissues and may be related to certain disease states.

Materials and Methods

Abs

Balb/c mice were purchased from Sankyo Lab Service (Tokyo). All animal protocols were approved by the Animal Care and Use Committee of Tokyo University of Science, and the experiments were performed in accordance with the RIBS Institutional Animal Care and Use Guidelines. Eight-wk-old BALB/c mice were immunized i.p. with 100 μg of HSA (Sigma) in complete Freund's adjuvant (WAKO) followed by repeated immunization with 100 μg of HSA in phosphate-buffered saline (PBS). Spleen cells from the mice were fused with Sp2/O cells using PEG1500 (Roche Applied Science). Hybridomas producing anti-HSA IgG mAbs were screened by ELISA using plates coated with HSA and horseradish-peroxydase-conjugated goat anti-mouse IgG Ab (SouthernBiotech).

The mAbs were purified from ascites using a column of HSA conjugated to Sepharose 4B (GE Healthcare). Ab concentrations were determined from UV absorption at 280 nm using a molar absorption coefficient, ε, of $2.1 \times 10^5\,M^{-1}\,cm^{-1}$. The anti-HSA Abs used in the present experiment were HAy1, HAy2, HAy3, HAy4 and HAy5.

HSA and its NEG

Fatty acid- and globulin-free grade HSA was purchased from Sigma. HSA dimers were eliminated using gel filtration chromatography with a HiPrep Sepharyl S-300 column (GE Healthcare). A value of $3.5 \times 10^4\,M^{-1}\,cm^{-1}$ was used as ε of the resulting monomeric HSA.

Non-enzymatic glycosylation of HSA *in vitro* was carried out essentially as previously described (*23–25*). The reaction was carried out by changing temperature, glucose concentration or reaction time. After the reaction, free glucose was removed by dialysis. We used an NEG HSA preparation, referred to gHSA. In order to obtain NGE preparations characteristic to AGE in terms of colour, *i.e.* absorption and fluorescence (*26*), we incubated HSA with 0.5 M glucose for 180 days at 37°C under sterile conditions. The molecular weights of the products were assessed using matrix-assisted laser desorption/ionization time-of-flight mass spectrometry (MALDI TOF MS) (Shimadzu) and the extent of NEG was estimated assuming that only the ketoamine adduct was conjugated to HSA. The molecular weights of the products were also estimated by SDS–PAGE. The protein concentrations of gHSA and AGE-HSA were determined using the same molar adsorption coefficient as for HSA.

MALDI TOF MS

The matrix solution contained 10 mg/ml 3,5-dimethoxy-4-hydroxycinnamic acid (sinapinic acid) in 60% v/v acetonitrile in 0.1% v/v aqueous trifluoroacetic acid. Sample protein solutions (1 μl of a 1 : 1 v/v mixture of 1 mg/ml total protein and matrix solution) were spotted on a steel plate slide and dried in a stream of warm air. The analyses were performed with a Shimadzu Biotech AXIMA TOF2 mass spectrometer set at positive high energy linear mode. Operation of the instrument, data collection and analysis were carried out according to the manufacturer's guidelines.

ITC

ITC experiments were carried out on a MicroCal VP-ITC isothermal titration calorimeter. Both mAbs and HSA or gHSA were dialysed against 50 mM phosphate containing 150 mM NaCl at varying pH values. All samples were carefully degassed before measurement. For forward titration, a 30 or 60 μM Ab solution was injected in 3 or 6 μl increments, respectively, into the HSA or gHSA solution (2 or 4 μM, respectively) at various temperatures. The heat of each injection was subtracted from the heat of dilution of the injectant, which was measured by adding the mAb solution to the buffer by injection. Each corrected heat value was divided by the moles of the HSA or gHSA injected and the data were analysed with Origin software (OriginLab). Reverse titration was carried out by injecting HSA into the mAb solution in the sample cell to assess the stoichiometry of the binding of the Ab to the Ag (*27*). The first data point was excluded from the analysis due to dilution within the injection needle and the cell.

To obtain the K_a and ΔH for the Ag–Ab interaction, a single set of identical binding sites was assumed and fitted to the resulting titration curves using a non-linear regression method. The Gibbs

free energy change, ΔG and ΔS were calculated from the following equation:

$$\Delta G = -RT\ln K_a = \Delta H - T\Delta S \quad (1)$$

where R is the gas constant and T is the absolute temperature in Kelvin.

ELISA

Binding of anti-HSA mAbs to HSA adsorbed on plastic plates was measured by ELISA within a pH range of 4–9.5. The buffers used were; acetate buffer (pH from 3.5 to 5.5), phosphate buffer (pH from 6.0 to 7.5) and carbonate buffer (pH from 8.0 to pH 9.5). The salt concentration was adjusted to 100 mM. The 96-well ELISA plates (NUNC) were coated with 1 μg/ml HSA in each buffer (50 μl/well). To compare pH-dependent binding, a fixed amount of mAb in different pH solutions was added to the wells. After a 2 h incubation, the wells were washed with PBS containing 0.1% Tween-20 (PBST) and the amount of Abs that had bound to the plates was estimated using goat anti-mouse IgG1 Abs conjugated to horseradish peroxydase (Abcam) with *o*-phenylenediamine substrate at a final concentration of 0.04% hydrogen peroxide in 0.1 M citrated buffer at pH 5.0. In some experiments, serially diluted mAbs at concentrations of 0.1 ng/ml to 10 μg/ml were incubated for 1 h and the Abs that had bound were estimated in a similar manner. The reaction was stopped by the addition of 50 μl/well of 1 M sulphuric acid. Colorimetric measurement was performed with a plate reader (BIORAD) at 490 nm.

For the competitive binding assay, HSA was biotinylated (HSA_{bio}) by reacting with the hydroxysuccinimide ester of biotin. A fixed amount of HSA_{bio} was mixed with various concentrations of gHSA and reacted with anti-HSA mAbs on the plates. After a 2-h incubation, the plates were washed with PBST. The bound HSA_{bio} was measured using horseradish-peroxidase-labelled streptavidin with o-phenylendiamine as described.

Circular dichroism measurements

Circular dichroism (CD) spectra were measured at 25°C with a Jasco J-720WI spectropolarimeter. The spectra were recorded and expressed as the mean residue ellipticity, [θ], which is defined as $[\theta] = (100 \times \theta_{obs})/(lc)$, where θ_{obs} is the observed ellipticity in degrees, c is the molar residue concentration of the protein calculated with a value of 107 for the mean residue molecular weight and l is the light path length in centimeters. Far-UV CD spectra were measured at a protein concentration of ~1.5 μM for HSA, gHSA and AGE-HSA using a 0.1 cm path length cell.

Yeast surface display

To obtain the full-length HSA gene from a human liver cDNA library (Takara), a nested PCR was performed using KOD-Plus-polymerase (TOYOBO) with the following primer sets: first PCR, 1.1sn and 6.1as and second PCR, 1.2sn and 6.2as (Supplementary Table S1). For expression of intact HSA in yeast, the resulting amplified HSA gene was cloned into the plasmid pCTNB (*28*) using *Sfi* I and *Not* I sites. For expression of truncated HSAs in yeast, gene fragments were amplified from the full-length HSA gene using the primers shown in Supplementary Table S1. The resulting amplified fragments were also cloned into pCTNB using *Sfi* I and *Not* I sites. A schema for the construction is shown in Fig. 1. pCTNB harboring the full-length HSA or truncated HSA gene was transfected into EBY100 yeast using a Frozen-EZ Yeast Transformation II kit (Zymo Research). Cells were cultivated on a synthetic dextrose medium with casamino acids (SD-CAA) plate at 30°C. After two days, single colonies were transferred to SD-CAA medium and cultivated at 30°C. After an overnight incubation, yeast cells were transferred and cultivated in SG-CAA medium at 20°C for 2 days. Grown cells were harvested and 1×10^7 yeast cells were used for FACS analysis. Cells were washed in FACS buffer (PBS with 0.5% BSA), then incubated with 50 μl FACS buffer containing each Ab (10 μg/ml) for 30 min on ice. The cells were washed and incubated with biotinylated goat anti-mouse IgG1 (Southern Biotech) for 30 min on ice. Cells were then washed and stained with 50 μl FACS buffer containing SA-PE (eBioscience) and FITC-conjugated rabbit anti-c-myc Abs (Abcam) for 30 min on ice and then washed and analysed by FACS Calibur (BD Bioscience) with CellQuest software supplied by the instrument vendor.

Results

Epitope mapping

HSA consists of three domains, DOM I, DOM II and DOM III (*1*, *29*). We divided these domains further into subdomains sDOM Ia, sDOM Ib, sDOM IIa, sDOM IIb, sDOM IIIa and sDOM IIIb (Fig. 1A). The plasmids encoding these subdomains and their various combinations in addition to whole HSA (Fig. 1B), were constructed using the primers listed in Supplementary Table S1 and were transfected into the EBY100 yeast strain. The expression of truncated genes was confirmed by detection of the anti-*c-myc* tag (data not shown).

The binding of anti-HSA mAbs to HSA or its fragments on the yeast was examined by flow cytometry (Fig. 2A). All mAbs bound to whole HSA on the yeast surface and these interactions were inhibited by free HSA in solution (data not shown). HAy1 bound to sDOM Ia, HAy3 to sDOM IIb and HAy5 to sDOM IIIb. Since HAy2 and HAy4 did not bind to a single subdomain, further analyses were performed using fused domains (Fig. 1B). HAy2 bound to DOM I + sDOM IIa but not to DOM I nor to DOM II + DOM III (Fig. 2B and C). HAy4 bound to DOM I + sDOM IIa in addition to DOM III but not to DOM I alone or to a fragment lacking DOM I, *i.e.* DOM II + DOM III. Therefore, it is likely that the HAy4 epitope consisted of DOM I + sDOM IIa and DOM III (Fig. 2B).

The epitopes of the respective mAbs, thus determined, are schematically presented using a 3D HSA model (Fig. 2D). They are grouped into two types: Type I mAbs, HAy1, HAy3 and HAy5, which recognized individual subdomains and Type II mAbs, HAy2 and HAy4, which recognized the epitope that expanded the structure and was composed of plural subdomains.

Thermodynamics of the interaction between Abs and HSA

The binding heat of anti-HSA mAbs in phosphate buffer at pH 7.4 was measured by ITC (Fig. 3). We performed the titration by adding each mAb solution in a syringe (injectant) to the HSA solution (forward titration). HAy1 and HAy2 were characterized by an endothermic heat, while HAy3, HAy4 and HAy5 by an exothermic heat. Therefore, it was likely that the sign of the reaction heat depended on the nature of the epitopes as well as on the mAb combining sites. The solid lines in the figure represent the best least-squares fit of the reaction heat per mole of injectant against the molar ratio, *i.e.* [Ab]/[HSA]. The thermodynamic parameters calculated using Eq. 1 are listed in Table I. Gibb's free energy was ~11–12 kcal/mol irrespective of the reaction heat sign, which provided K_a values in a range of 10^7 to $10^9\ M^{-1}$. Similar results were obtained when the titration was performed using the HSA solution as injectant (reverse titration). Enthalpy–entropy compensation at pH 7.4 in the binding of mAbs to HSA is plotted in Fig. 3F. The linear 0.98 slope indicated that the anti-HSA mAbs were characterized by a correlation typical of thermodynamic compensation,

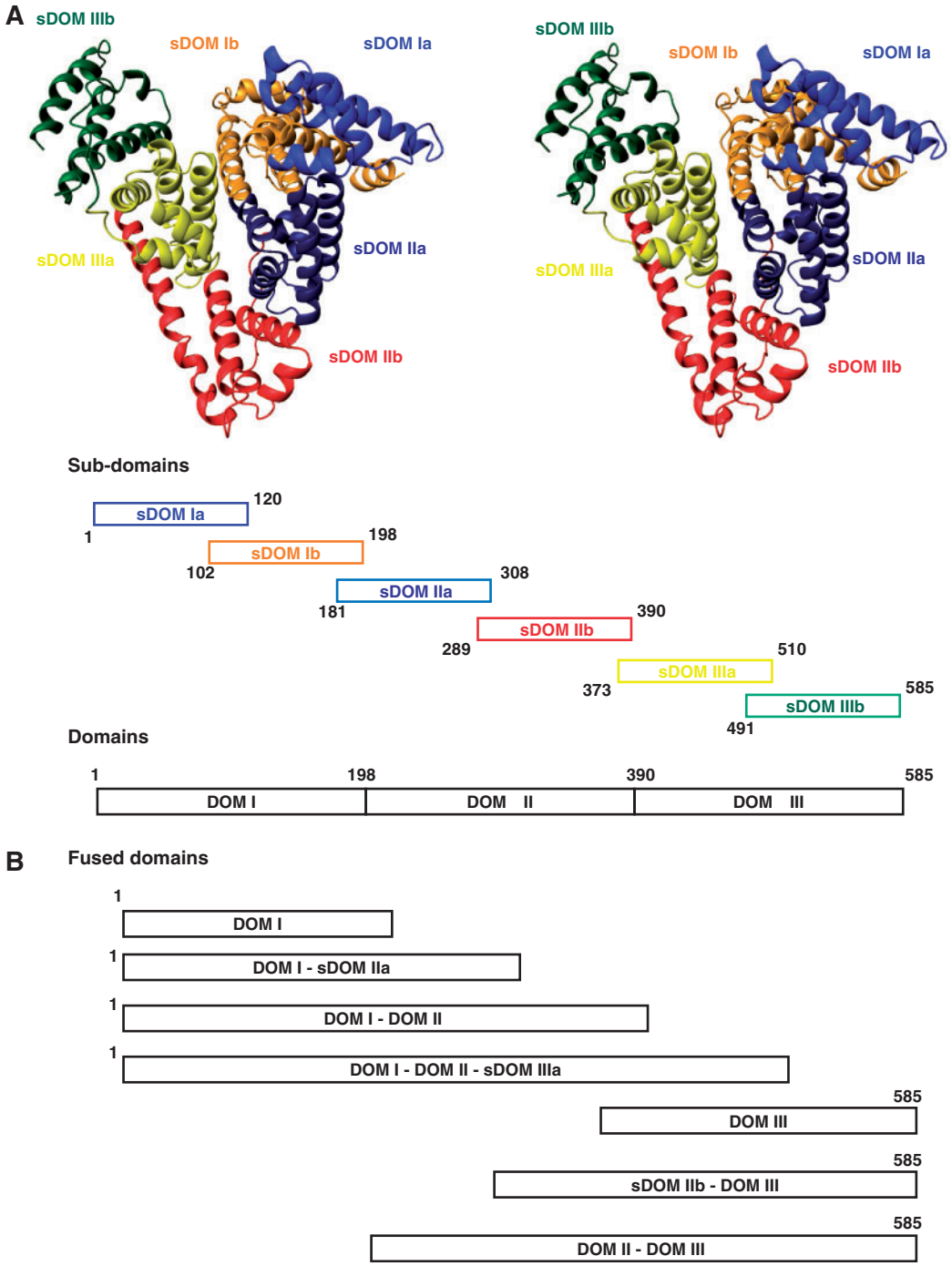

Fig. 1 The domain structure of HSA and its fragments displayed on the yeast surface. (A) Stereoview of HSA shown in a ribbon representation coloured according to subdomains referred to as sDOM Ia, sDOM Ib, sDOM IIa, sDOM IIb, sDOM IIIa and sDOM IIIb. The domains designated DOM I, DOM II and DOM III are also represented. (B) The DNA fragments encoding various combinations of subdomains or domains, referred to as fused domains, in addition to full-length HSA were generated by PCR using specific primers listed in Supplementary Table S1 for epitope mapping by use of YSD.

which has been consistently observed in Ag–Ab interactions and explained in terms of water reorganization (*30*).

pH-dependent interaction between HSA and anti-HSA mAbs

The interaction of mAbs with HSA coated on the plastic plates was measured at various pH values by ELISA. Coating of plates with HSA and subsequent reaction with the mAbs were carried out at the same pH. Percentages of binding relative to the maximum binding at pH 6.0 were plotted against pH (Fig. 4A). HAy5 showed no significant change in binding over a pH range of 4–9, suggesting that the subdomain, sDOM IIIb, recognized by this mAb has a stable conformation over this pH range. The mAbs HAy3 and HAy4 showed a decrease in binding below pH 5. This may correspond to an N-F transition which

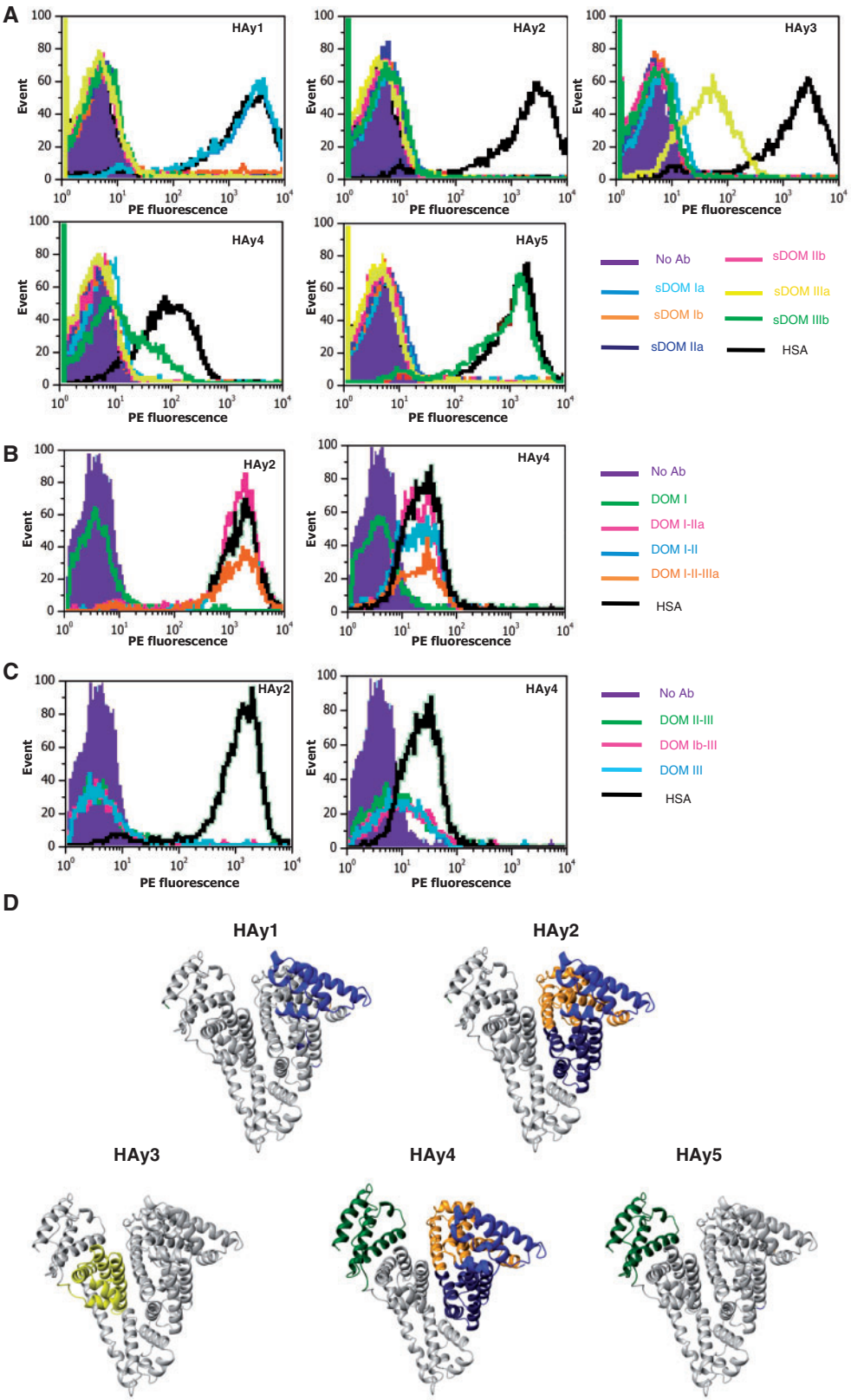

Fig. 2 Interaction of anti-HSA Abs with HSA fragments expressed on the yeast surface. (A) Yeast cells were stained using anti-c-myc Ab conjugated with FITC, and anti-HSA mAbs bound to the cells were stained using rabbit anti-mouse IgG1 Ab conjugated with phycoerythrin (PE). PE fluorescence intensities of the gated fraction of c-myc-tag-expressing cells (FITC-positive cells) are shown. The open histograms show the binding of five anti-HSA mAbs to yeast cells expressing the respective subdomains coloured as indicated and full-length HSA (black). The filled histogram is a control without Ab staining. (B) The binding of HAy2 (left) and HAy4 (right) to HSA fragments with deleted carboxyl terminal subdomains. (C) The binding of HAy2 (left) and HAy4 (right) to HSA fragments with deleted amino terminal domains. The designation of the HSA fragments is shown in Fig 1. (D) Schematic representation of the epitopes in a 3D structure model. The epitopes recognized by respective mAbs are coloured. The graphics were rendered using the molecular visualization software MOLMOL (*35*).

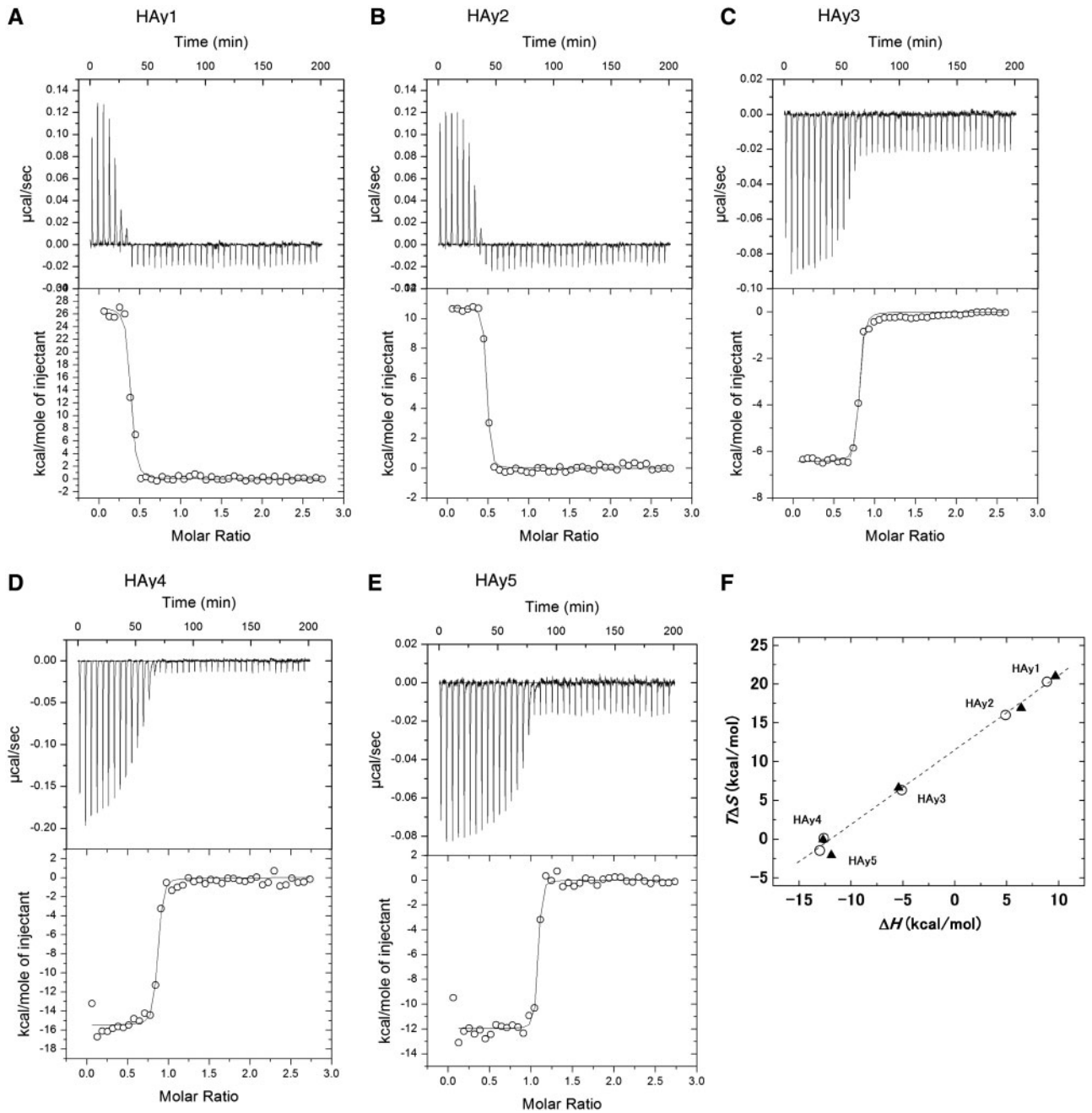

Fig. 3 ITC measurements for the binding of anti-HSA Abs to HSA and enthalpy versus entropy compensation plots. (A–E) Top, Forward titrations were performed by injecting the mAb solution into the HSA solution at pH 7.4 and 25°C. Bottom, Integration of the binding heats was plotted against molar ratios from the raw data. The mAb used for each measurement is indicated in each panel. Fitted curves are shown as a solid line, and were obtained by fitting to a one equivalent binding site model. (F) The ΔH values are plotted against the $T\Delta S$ obtained from forward ITC (open circle) and reverse ITC (filled triangle). The slope (dashed line), which was calculated by linear regression fitting, was 0.98.

accompanies the conformational change in the epitopes recognized by these mAbs. HAy2 and HAy4 showed pH-dependent binding at acidic, neutral and basic pH, although the change at a neutral to basic pH of HAy4 was smaller with HAy4 than with HAy2. pH-dependent binding at pH 4 would correspond to an N-F transition as described above and that at pH 7–9, to an N-B transition (Fig. 4A).

The binding of each mAb to HSA at a pH above 6.0 was examined in detail (Fig. 4B) by changing Ab concentrations. HAy2 showed a significant decrease in binding on increasing the pH to within a range of 6.0–9.5. Although the difference in the binding of HAy4 was rather small compared with HAy2, it was still significant, while no difference was observed in the binding of the other mAbs. While ELISA is convenient for measuring Ag–Ab interactions, it may not be appropriate for describing the thermodynamics of protein–protein interactions since either the Ag or Ab has to be immobilized on the plate. Therefore, we examined interactions between HSA and mAbs by ITC.

Table I. Thermodynamic parameters for binding of anti-HSA mAbs to HSA at pH 7.4.

mAbs	K_a (M^{-1})	ΔG (kcal mol^{-1})	ΔH (kcal mol^{-1})	ΔS^a (cal $mol^{-1}K^{-1}$)	$T\Delta S^a$ (kcal mol^{-1})
Titration of mAb into HSA					
HAy1	$1.9 \pm 0.9 \times 10^8$	−11.3	8.9 ± 0.22	67.6	20.2
HAy2	$1.5 \pm 0.3 \times 10^8$	−11.1	4.9 ± 0.04	53.8	16.0
HAy3	$2.3 \pm 0.5 \times 10^8$	−11.5	−5.1 ± 0.05	21.3	6.4
HAy4	$2.7 \pm 0.9 \times 10^8$	−11.5	−13.0 ± 0.17	−5.0	−1.5
HAy5	$2.1 \pm 0.2 \times 10^9$	−12.7	−12.6 ± 0.21	0.4	0.1
Titration of HSA into mAb					
HAy1	$2.2 \pm 0.9 \times 10^8$	−11.4	9.2 ± 0.17	69.1	20.6
HAy2	$1.1 \pm 0.3 \times 10^8$	−11.0	5.0 ± 0.09	53.5	16.0
HAy3	$1.6 \pm 0.8 \times 10^8$	−11.2	−5.9 ± 0.15	17.7	5.3
HAy4	$1.5 \pm 0.4 \times 10^7$	−9.8	−11.9 ± 0.39	−7.1	−2.1
HAy5	$1.2 \pm 0.7 \times 10^9$	−12.4	−12.9 ± 0.18	−1.5	−0.5

[a]The values were calculated from the equation $\Delta G = \Delta H - T\Delta S$.

The ΔH values in the reaction between HAy2 or HAy1 and HSA are plotted against pH in Fig. 4C and D, respectively. Although only a small variation in ΔH was observed with HAy1 between pH 5.0 and 8.0, a sharp decrease above pH 7.5 was characteristic of HAy2.

Preparation and characterization of gHSA and AGE-HSA

We carried out the NEG reaction *in vitro* under various experimental conditions. The MW was analysed by SDS–PAGE (Fig. 5A) and MALDI TOF MS (Fig. 5B). Although no significant change in the mobility of gHSA was observed, AEG-HSA showed a slow and broad band on SDS–PAGE. The MS spectra of HSA, gHSA and AGE-HSA gave a single peak, corresponding to a molecular mass of 66,275 ± 79 for HSA, 68,249 ± 269 for gHSA and 73,409 ± 488 for AGE-HSA (Table II). Since NEG of HSA was known to occur at approximately 10 sites *in vivo* (*31*), we used this preparation as representative of the early NEG product.

Figure 5C shows the far-UV CD spectra of HSA, gHSA and AGE-HSA, which reflect the secondary and tertiary structure of the protein. HSA was shown to have a helical structure with an α-helix content of 65% (*3*) and negative maxima at 208 and 222 nm were considered to have arisen from the α-helices. No significant difference between spectra of HSA and gHSA was observed, indicating that the contribution of sugar adducts to CD spectrum was negligible (*13*) and that NEG has little effect on the secondary or tertiary structure of HSA at an early stage of glycosylation. However, the CD spectrum of AGE-HSA was significantly different from those of HSA and gHSA, suggesting changes in the secondary and tertiary structure.

Interaction of anti-HSA mAbs with NEG-HSA

Figure 6 shows the binding competition of HSA, gHSA and AGE-HSA to mAbs coated on the ELISA plates. The binding of biotin-labelled HSA, HSA_{bio}, to the respective mAbs was inhibited with non-labelled HSA, gHSA and AGE-HSA in a concentration-dependent manner. Virtually identical inhibition curves were obtained for HSA and gHSA, indicating that none of the mAbs were able to recognize a structural difference between HSA and gHSA. Therefore, it was suggested that the glycation of ε-amino groups of the lysine residues did not induce steric hindrance or conformational change in the HSA structure of the early stage NEG products. On the other hand, AGE-HSA showed little inhibition in binding to HAy2 and a 100-fold lower inhibition in binding to HAy3 compared with HSA, indicating that the structure recognized by HAy2 and HAy3 was altered considerably by glycation, although it was capable of binding to HAy1. These results indicated that the structure of sDOM I, which was recognized by HAy1, remained unchanged, while the other structures including subdomains and structures created by interdomain interactions were altered greatly.

Thermodynamic measurements in the interaction between gHSA and HAy2

Anti-HSA mAbs failed to detect any difference in structure between HSA and gHSA on ELISA. Therefore, we examined whether NEG had little effect on the HSA–Ab interaction in terms of thermodynamics as measured by ITC. The results showed that the reaction of HAy2 with gHSA was endothermic, similar to that with HSA, and that the difference of ΔH values in the reaction of HAy2 with gHSA and HSA ($\Delta\Delta H^{gHSA-HSA}$ in Table III) became negative. Since a positive ΔH contributes unfavourably to the binding free energy change, it was clear that glycation had a favourable effect on the HSA–Ab interaction through a decrease in the positive ΔH values with HAy2. The other mAbs, HAy1 and HAy3, did not show a significant change in ΔH value. In spite of the favourable contribution of ΔH on glycation, the difference in Gibb's free energy between the interaction with HSA and gHSA became negligible due to an increase in the unfavourable ΔS value caused by enthalpy–entropy compensation. This would explain why we could not detect a difference in binding between HSA and gHSA on ELISA. The results indicated that glycosylation of lysine residues did not provide steric hindrance but rather enhanced the Ab-HSA non-covalent interaction.

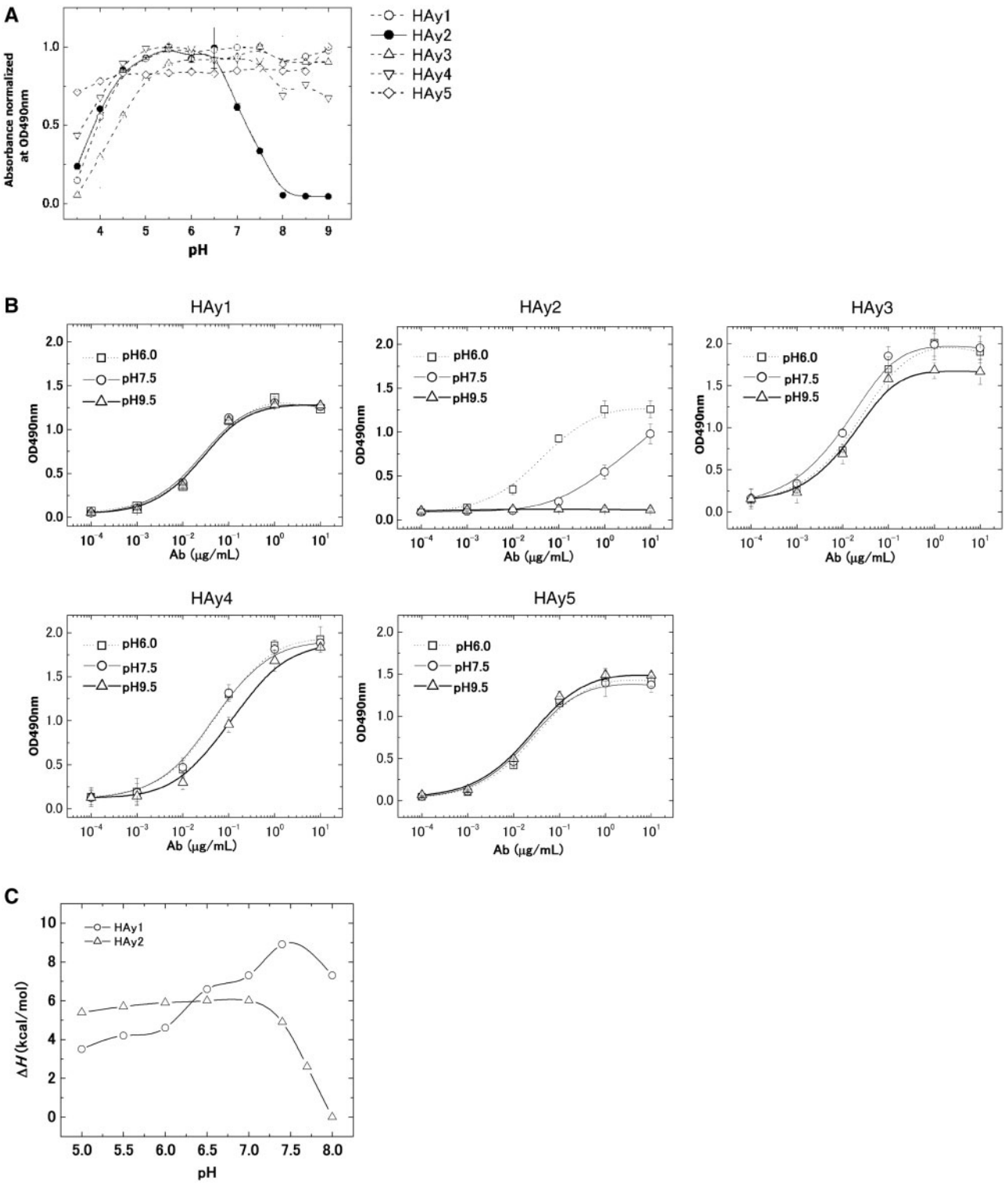

Fig. 4 pH-dependent binding of anti-HSA mAbs to HSA. (A) Binding of mAbs at a fixed concentration to HSA coated on the ELISA plates was measured at various pH values. The ordinate provides the ratio of binding relative to the maximum binding at pH 6. (B) The concentration-dependent profiles of mAbs in binding to HSA at pH 6, 7.5 and 9. Measurements were performed in duplicate. Standard deviations are shown as error bars. (C) Effects of pH on ΔH obtained from ITC measurements of HAy2 and HAy1, respectively.

Discussion

DNA nucleotide sequences (*1*) predicted that HSA was composed of subdomains, each with a minimal structural unit of ~120 amino acid residues. Although HSA was shown to consist of three domains, DOM I, DOM II and DOM III, by preparing each domain as a recombinant protein (*29*), independent folding of the subdomains has not been verified at the protein level.

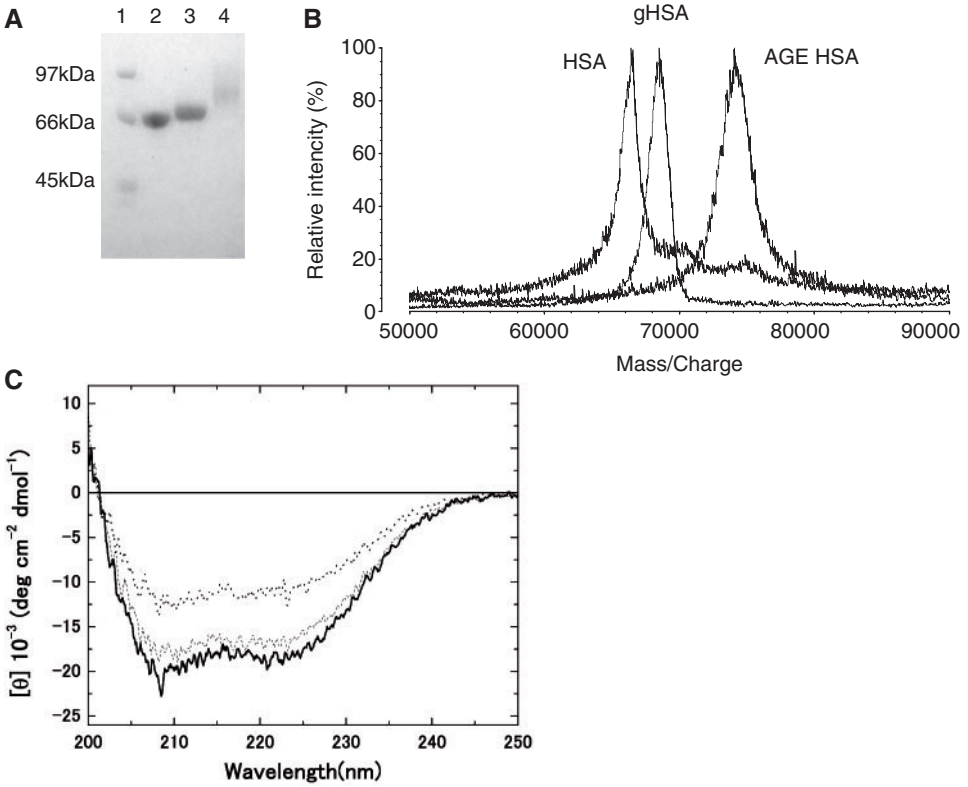

Fig. 5 Characterization of the molecular properties of gHSA and AGE-HSA. (A) SDS–PAGE analysis. Lane 1, MW marker; lane 2, HSA; lane 3, gHSA and lane 4, AGE-HSA. (B) MULDI TOF MS spectra of HSA, gHSA and AGE-HSA. (C) Far-UV CD spectra of HSA, gHSA and AEG-HSA. Solid line, HSA; broken line, gHSA; dotted line, AGE-HSA.

Table II. Molecular mass of HSA and gHSA.

Sample	Molecular mass[a] Mean ± SE	Increased mass	Number of NEG[b]
HSA	66,275 ± 79	0	0
gHSA	68,249 ± 269	+1974	12
AGE-HSA	73,409 ± 488	+7134	44

[a]Molecular mass values are averages of ten experiments by MALDI TOF Mass measurements. [b]Number of NEG was calculated assuming adducts of fructosyl groups with MW of 162.

In the present study, we expressed each subdomain on the yeast surface as well as various combinations of subdomains, domains and full-length HSA, and their expression was confirmed by the binding of specific Ab to the c-myc tag. Using these yeast-surface-expressed HSA fragments, we identified the epitopes of three mAbs, HAy1, HAy3 and HAy5, as being the subdomains sDOM Ia, sDOM IIb and sDOM IIIb, respectively. Two other mAbs, HAy2 and HAy4, did not react with any single subdomain but instead bound to fragments consisting of plural subdomains, suggesting that these mAbs recognized a complex structure resulting from intersubdomain interactions. This information on the epitopes in relation to the 3D protein structure was vital to our purpose, i.e. showing the utility of mAbs in detecting conformational changes in proteins, and the fact that the epitopes were so well-characterized certainly contributed to our success. YSD has also been effectively used for epitope mapping of other proteins such as botulinum neurotoxin (*19*) and epidermal growth factor (*18*).

ITC provides information on Ag–Ab interactions through the measurement of such thermodynamic parameters as ΔH and K_a. From these, one can calculate ΔG and ΔS. In our experiments, the values obtained in this manner varied widely among the mAbs (Table I). An endothermic heat was observed in reactions with HAy1 and HAy2, which indicates that these reactions were entropy-driven. On the other hand, three mAbs had reactions that were exothermic and enthalpy-driven. Whichever the ΔH sign, the plots of ΔH versus $T\Delta S$ provided a straight line with a slope of 0.982, suggesting that ΔH and $T\Delta S$ compensated for each other. This was a widely observed phenomenon in the Ag–Ab interactions.

We used the anti-HSA mAbs to identify which domains were involved in the conformational transitions. HAy5 showed little pH dependence in binding to HSA, suggesting that sDOM IIIb, which is recognized by this mAb, is involved in neither an N-F nor N-B transition. On the other hand, HAy1, HAy2, HAy3 and HAy4 showed a decrease in binding below pH 5. Therefore, an N-F transition accompanied the conformation change in sDOM Ia and sDOM IIb, although a decrease in the binding activity due to acid denaturation of the mAbs themselves has to be considered (*31*). Three mAbs, HAy1, HAy3 and HAy5, bound to sDOM Ia, sDOM IIb and sDOM IIIb, respectively, but did not show pH-dependent

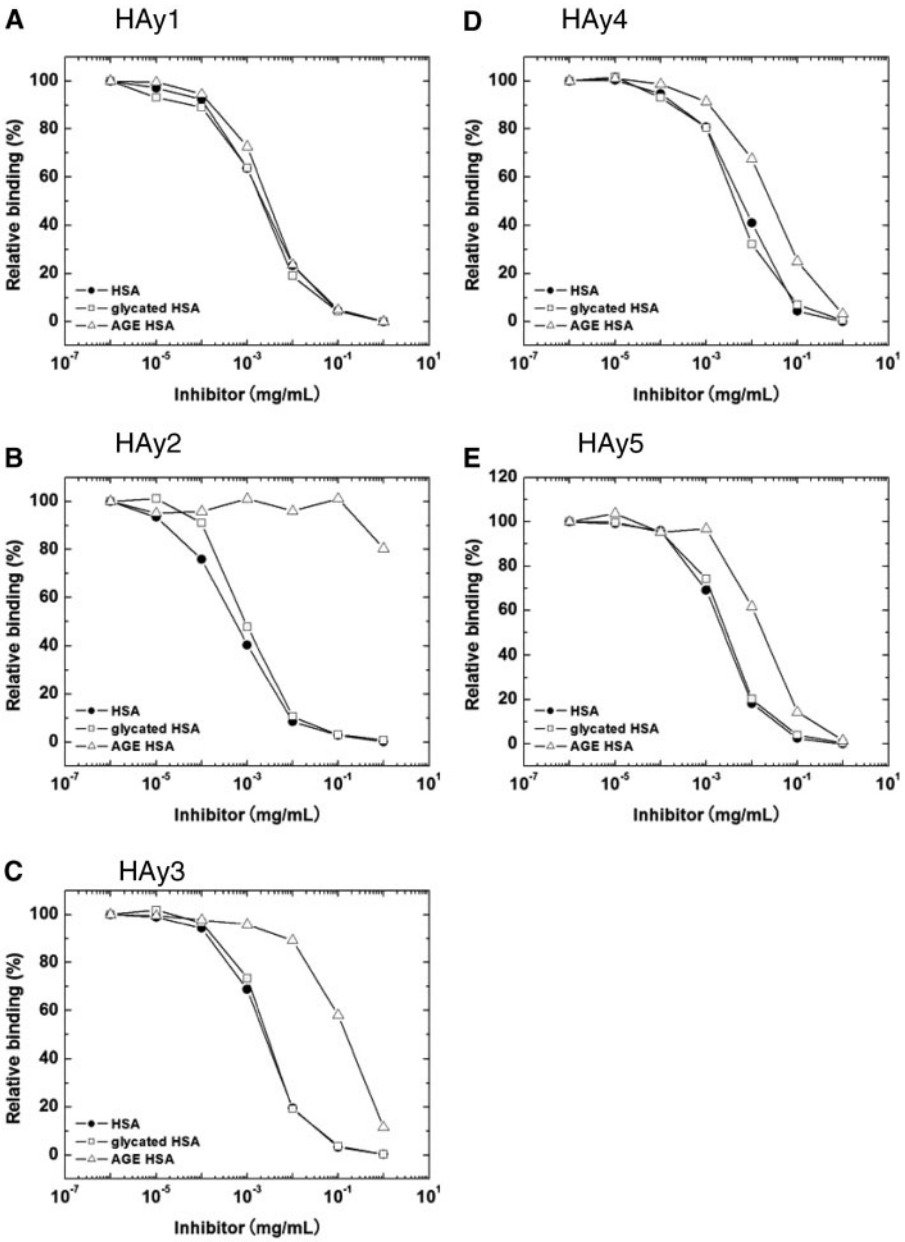

Fig. 6 Competitive binding of HSA and gHSA to anti-HSA mAbs coated on the ELISA plates. Biotin-labelled HSA, HSA_{bio}, was used as a detecting Ag, and non-labelled HSA, gHSA and AEG-HSA were used as competitors. The amount of bound HSA_{bio} was measured using peroxidase-labelled streptavidin. Closed circle, HSA; open circle, gHSA; open square, AGE-HSA.

binding above pH 7, indicating that these subdomains did not participate in an N-B transition. However, HAy2 showed a sharp decrease in binding above pH 7. HAy4 also showed a decrease in binding within a similar pH range, although the magnitude of the change was small compared with HAy2. Since the HAy2 epitope was determined to be DOM I-sDOM IIa and that of HAy4 to be DOM I-DOM III, these two mAbs are likely to recognize an epitope created by an interaction of plural subdomains and not a single subdomain. Therefore, we concluded that an N-B transition occurs when accompanied by a rearrangement in the conformation around DOM I. These findings are in good agreement with results reported by Bos *et al.* (*21*).

Glycated HSA accounts for 80% of the circulating glycated protein and it has been implicated in several complications associated with diabetes (*12*). Amadori glucose adducts of HSA were shown to stimulate the production of Type IV collagen by mesangial cells in culture (*32*). The effect of NEG on the binding of long fatty acids was also shown by Shaklai *et al.* (*33*). HSA possesses 58 Lys residues (*1*) which can potentially undergo NEG on their side chains, although it was shown that there are four main sites and several additional sites for NEG (*34*). MALDI TOF MS analysis revealed various products whose lysine and arginine side chains were converted to complicated structures in AGE-HSA (*11*). We addressed the question of whether such modification of amino acid side chains

Table III. Thermodynamic parameters for binding of anti-HSA mAbs to gHSA.

	Type I		Type II
	HAy1	HAy3	HAy2
K_a	$1.1 \pm 0.7 \times 10^8$	$8.5 \pm 0.3 \times 10^7$	$1.1 \pm 0.7 \times 10^8$
ΔG	−11.0	−10.8	−11.0
$\Delta\Delta G^{gHSA-HSA}$	0.8	0.7	0
ΔH^{gHSA}	7.8 ± 0.3	-4.8 ± 0.1	1.2 ± 0.03
$\Delta\Delta H^{gHSA-HSA}$	0.5	−0.3	−3.4
ΔS^{gHSAa}	62.9	20.1	40.9
$T\Delta S^{gHSAa}$	18.8	6.0	12.2
$T\Delta\Delta S^{gHSA-HSA}$	−0.3	−3.4	−1.0

All values are reported with the units in kcal mol^{-1} except for K_a which is in M^{-1} and ΔS which is in cal $mol^{-1}K^{-1}$.
[a]The values were calculated from the equation $\Delta G = \Delta H - T\Delta S$.

by NEG induces conformational changes, such as alteration of domain–domain interactions, using anti-HSA mAbs capable of detecting conformational changes in HSA induced by varying the pH. Since the gHSA preparations were stable in neutral pH solutions, we considered that they were converted from the aldimine to ketoamine form through Amadori transition. However, no significant difference in the interaction of HSA or gHSA with the anti-HSA mAbs was detected by ELISA, suggesting that the ketoamine adducts provided no steric hindrance and induced no gross structural changes in HSA. This coincided with the results of CD measurements; no change was observed in the CD spectra below 250 nm which reflects the back bone conformation of proteins [Fig. 5, (*13*)]. However, the ITC analysis revealed that the positive ΔH values decreased in interactions between HAy2 and gHSA compared with those with HSA (Table III). This change in the ΔH value brought about a favourable effect on the ΔG but was compensated for by an increase in the unfavourable ΔS.

A favourable effect on ΔH with sugar adducts suggested that they provided little structural hindrance but rather contributed to strengthening the Ab–Ag interaction. This might be due to an increase in hydrophobic interactions by conversion of positively charged ε-amino groups to aldimine or ketoamine adducts with no charged groups. Previously, the intrinsic tryptophan fluorescence of HSA was shown to be quenched by NEG (*25*, *33*), indicating that the microenvironment around Trp214 was altered. Collectively, the structure of the early stages NEG products was similar to that of intact HSA, although the nature of the protein surface varied slightly.

In contrast to its interaction with gHSA, HAy2 was unable to bind to AGE-HSA. The mAbs HAy3, HAy4 and HAy5 also showed a decrease in binding to AGE-HSA compared to HSA, although HAy1 did not. Judging from these mAb reactions, the AGE-HSA epitopes were significantly altered by glycation, which would be due to the change in the tertiary structure rather than to steric hindrance of the sugar adducts, since they had a tendency to strengthen the Ag–Ab interaction as described. We assume a structural model for AGE-HSA in which one or two subdomains retain a structure similar to that of HSA, while other subdomains unfold partially and intersubdomain interactions are prevented. This model is similar to that proposed for HSA isomers referred to as F and E forms (*1*). Based on the measurements of CD spectra, viscosity, and fluorescence spectra, Sattarahmady *et al.* (*14*) suggested that AGE-HSA has a structure that assumes a molten globule-like state.

In the present study, we showed that fine conformational changes in the HSA molecule can be detected by anti-HSA mAbs and that Abs provide a powerful tool for studying the conformation of a protein when its epitopes are defined on the 3D structure. HSA undergoes various natural modifications such as glycation by glucose, or alkylation by 4-hydroxy-2-nonenal. These modifications may induce conformational changes in HSA that are detectable by Abs and these changes may be related to certain diseases.

Supplementary Data

Supplementary data are available at *JB* Online.

Acknowledgements

The authors thank Dr K. Dane Wittrup (Massachusetts Institute of Technology) for providing the plasmid pCTNB and Dr Hirokazu Furue (Tokyo University of Science) for use of the CD spectrometer.

Conflict of Interest
None declared.

References

1. Carter, D.C. and Ho, J.X. (1994) Structure of serum albumin. *Adv. Protein Chem.* **45**, 153–203
2. He, X.M. and Carter, D.C. (1992) Atomic structure and chemistry of human serum albumin. *Nature*. **358**, 209–215
3. Minghetti, P.P., Ruffner, D.E., Kuang, W.J., Dennison, O.E., Hawkins, J.W., Beattie, W.G., and Dugaiczyk, A. (1986) Molecular structure of the human albumin gene is revealed by nucleotide sequence within q11-22 of chromosome 4. *J. Biol. Chem.* **261**, 6747–6757
4. Sugio, S., Kashima, A., Mochizuki, S., Noda, M., and Kobayashi, K. (1999) Crystal structure of human serum albumin at 2.5 A resolution. *Protein Eng.* **12**, 439–446
5. Varshney, A., Sen, P., Ahmad, E., Rehan, M., Subbarao, N., and Khan, R.H. (2010) Ligand binding strategies of human serum albumin: how can the cargo be utilized? *Chirality*. **22**, 77–87
6. Ghuman, J., Zunszain, P.A., Petitpas, I., Bhattacharya, A.A., Otagiri, M., and Curry, S. (2005) Structural basis of the drug-binding specificity of human serum albumin. *J. Mol. Biol.* **353**, 38–52
7. Petitpas, I., Bhattacharya, A.A., Twine, S., East, M., and Curry, S. (2001) Crystal structure analysis of warfarin binding to human serum albumin: anatomy of drug site I. *J. Biol. Chem.* **276**, 22804–22809
8. Simard, J.R., Zunszain, P.A., Hamilton, J.A., and Curry, S. (2006) Location of high and low affinity fatty acid binding sites on human serum albumin revealed by NMR drug-competition analysis. *J. Mol. Biol.* **361**, 336–351
9. Zunszain, P.A., Ghuman, J., Komatsu, T., Tsuchida, E., and Curry, S. (2003) Crystal structural analysis of human

serum albumin complexed with hemin and fatty acid. *BMC Struct. Biol.* **3**, 6
10. Urbanowski, J.C., Cohenford, M.A., and Dain, J.A. (1982) Nonenzymatic galactosylation of human serum albumin. In vitro preparation. *J. Biol. Chem.* **257**, 111–115
11. Wa, C., Cerny, R.L., Clarke, W.A., and Hage, D.S. (2007) Characterization of glycation adducts on human serum albumin by matrix-assisted laser desorption/ionization time-of-flight mass spectrometry. *Clin. Chim. Acta* **385**, 48–60
12. Cohen, M.P. (2003) Intervention strategies to prevent pathogenetic effects of glycated albumin. *Arch. Biochem. Biophys.* **419**, 25–30
13. Mendez, D.L., Jensen, R.A., McElroy, L.A., Pena, J.M., and Esquerra, R.M. (2005) The effect of non-enzymatic glycation on the unfolding of human serum albumin. *Arch. Biochem. Biophys.* **444**, 92–99
14. Sattarahmady, N., Moosavi-Movahedi, A.A., Ahmad, F., Hakimelahi, G.H., Habibi-Rezaei, M., Saboury, A.A., and Sheibani, N. (2007) Formation of the molten globule-like state during prolonged glycation of human serum albumin. *Biochim. Biophys. Acta* **1770**, 933–942
15. Oda, M., Kitai, A., Murakami, A., Nishimura, M., Ohkuri, T., Abe, Y., Ueda, T., Nakamura, H., and Azuma, T. (2010) Evaluation of the conformational equilibrium of reduced hen egg lysozyme by antibodies to the native form. *Arch. Biochem. Biophys.* **494**, 145–150
16. Sachs, D.H., Schechter, A.N., Eastlake, A., and Anfinsen, C.B. (1972) An immunologic approach to the conformational equilibria of polypeptides. *Proc. Natl. Acad. Sci. USA* **69**, 3790–3794
17. Petersen, C.E., Ha, C.E., Curry, S., and Bhagavan, N.V. (2002) Probing the structure of the warfarin-binding site on human serum albumin using site-directed mutagenesis. *Proteins* **47**, 116–125
18. Chao, G., Cochran, J.R., and Wittrup, K.D. (2004) Fine epitope mapping of anti-epidermal growth factor receptor antibodies through random mutagenesis and yeast surface display. *J. Mol. Biol.* **342**, 539–550
19. Levy, R., Forsyth, C.M., LaPorte, S.L., Geren, I.N., Smith, L.A., and Marks, J.D. (2007) Fine and domain-level epitope mapping of botulinum neurotoxin type A neutralizing antibodies by yeast surface display. *J. Mol. Biol.* **365**, 196–210
20. Ladbury, J.E. and Chowdhry, B.Z. (1996) Sensing the heat: the application of isothermal titration calorimetry to thermodynamic studies of biomolecular interactions. *Chem. Biol.* **3**, 791–801
21. Bos, O.J., Labro, J.F., Fischer, M.J., Wilting, J., and Janssen, L.H. (1989) The molecular mechanism of the neutral-to-base transition of human serum albumin. Acid/base titration and proton nuclear magnetic resonance studies on a large peptic and a large tryptic fragment of albumin. *J. Biol. Chem.* **264**, 953–959
22. Furth, A.J. (1988) Methods for assaying nonenzymatic glycosylation. *Anal Biochem.* **175**, 347–360
23. Lapolla, A., Gerhardinger, C., Baldo, L., Fedele, D., Keane, A., Seraglia, R., Catinella, S., and Traldi, P. (1993) A study on in vitro glycation processes by matrix-assisted laser desorption ionization mass spectrometry. *Biochim. Biophys. Acta* **1225**, 33–38
24. Thornalley, P.J., Argirova, M., Ahmed, N., Mann, V.M., Argirov, O., and Dawnay, A. (2000) Mass spectrometric monitoring of albumin in uremia. *Kidney Int.* **58**, 2228–2234
25. Zoellner, H., Hou, J.Y., Hochgrebe, T., Poljak, A., Duncan, M.W., Golding, J., Henderson, T., and Lynch, G. (2001) Fluorometric and mass spectrometric analysis of nonenzymatic glycosylated albumin. *Biochem. Biophys. Res. Commun.* **284**, 83–89
26. Pongor, S., Ulrich, P.C., Bencsath, F.A., and Cerami, A. (1984) Aging of proteins: isolation and identification of a fluorescent chromophore from the reaction of polypeptides with glucose. *Proc. Natl. Acad. Sci. USA* **81**, 2684–2688
27. Velazquez-Campoy, A. and Freire, E. (2006) Isothermal titration calorimetry to determine association constants for high-affinity ligands. *Nat. Protoc.* **1**, 186–191
28. Boder, E.T. and Wittrup, K.D. (1997) Yeast surface display for screening combinatorial polypeptide libraries. *Nat. Biotechnol.* **15**, 553–557
29. Dockal, M., Carter, D.C., and Ruker, F. (1999) The three recombinant domains of human serum albumin. Structural characterization and ligand binding properties. *J. Biol. Chem.* **274**, 29303–29310
30. Swaminathan, C.P., Animesh, N., Visweswariah, S.S., and Surolia, A. (1999) Thermodynamic analyses reveal role of water release in epitope recognition by a monoclonal antibody against the human guanylyl cyclase C receptor. *J. Biol. Chem.* **274**, 31272–31278
31. Azuma, T., Hamaguchi, K., and Migita, S. (1972) Acid denaturation of Bence Jones proteins. *J. Biochem.* **71**, 379–386
32. Cohen, M.P., Wu, V.Y., and Cohen, J.A. (1997) Glycated albumin stimulates fibronectin and collagen IV production by glomerular endothelial cells under normoglycemic conditions. *Biochem. Biophys. Res. Commun.* **239**, 91–94
33. Shaklai, N., Garlick, R.L., and Bunn, H.F. (1984) Nonenzymatic glycosylation of human serum albumin alters its conformation and function. *J. Biol. Chem.* **259**, 3812–3817
34. Iberg, N. and Fluckiger, R. (1986) Nonenzymatic glycosylation of albumin in vivo. Identification of multiple glycosylated sites. *J. Biol. Chem.* **261**, 13542–13545
35. Koradi, R., Billeter, M., and Wuthrich, K. (1996) MOLMOL: a program for display and analysis of macromolecular structures. *J. Mol. Graph.* **14**, 51–55, 29–32